

PARAMETRIC STUDIES OF IMAGE-CHARGE EFFECTS IN SMALL-APERTURE ALTERNATING-GRADIENT FOCUSING SYSTEMS *

Jing Zhou[#] and Chiping Chen, Plasma Science and Fusion Center, MIT, Cambridge, MA 02139

Abstract

Image charges have important effects on an intense charged-particle beam propagating through an alternating-gradient (AG) focusing channel with a small circular aperture. This is especially true with regard to chaotic particle motion, halo formation, and beam loss. In this paper, we examine the dependence of these effects on system parameters such as the filling factor of the AG focusing field, the vacuum phase advance, the beam perveance, and the ratio of the beam size to the aperture. We calculate the percentage of beam loss to the conductor wall as a function of propagating distance and aperture, and compare theoretical results with simulation results from the particle-in-cell (PIC) code PFB2D.

INTRODUCTION

Alternating-gradient accelerators with high average power and high brightness beams are being constructed or proposed for basic scientific research such as heavy ion fusion, high-energy physics, high-energy density physics, and spallation neutron sources. An important aspect in the design of periodically focused beams in such accelerators and rf drivers for the next linear collider (NLC) is to prevent the beams from developing halos and chaos which may cause beam losses [1] to the conducting walls of the accelerating structures [3-9]. The problem of halo formation and beam losses is of a serious concern in the design of small-aperture focusing transport systems [10, 11] that are often required in order to keep accelerator costs manageable.

Two key mechanisms for halo formation: namely, mismatch in a constant focusing channel [3] and nonuniformity in an alternative-gradient focusing channel [5], have been studied using analytical models [3-5] and self-consistent simulations with particle-in-cell (PIC) [6-8] and Green's function techniques. A new mechanism for chaotic particle motion and halo formation due to the image-charge effects in intense charged-particle beams has been reported recently [1].

In the test-particle model [1], an rms-matched continuous intense charged-particle beam has been considered propagate in the longitudinal direction through an AG quadrupole magnetic field in a perfectly conducting round pipe with radius R . The beam density has been assumed to be uniform inside the beam ellipse $x^2/a^2 + y^2/b^2 = 1$. An analytical expression for the scalar potential has been obtained for the assumed density profile, and the periodic beam envelope functions $a(s) = a(s+S)$ and $b(s) = b(s+S)$ have been calculated

*Work supported by the U.S. DOE, Office of HEP, DE-FG02-95ER40919, Office of FES, DE-FG02-01ER54662, and in part by Air Force Office of Scientific Research, F49620-03-1-0230.

[#]jea_zhou@mit.edu

from the envelope equations [11]. In the paraxial approximation, the transverse equations of motion for an individual test particle have been obtained [1].

To demonstrate the image-charge effects on the particle motion and beam dynamics, a test-particle model has been used for the Kapchinskij-Vladimirskij (KV) beam distribution in a system with quadrupole focusing lattices of a periodic step-function with occupancy $\eta = 0.5$, perveance $KS/\varepsilon_x = 10.0$, emittance $\varepsilon_x = \varepsilon_y = \varepsilon$ and vacuum phase advance $\sigma_v = 80^\circ$, which correspond to those in the High-Current Experiment (HCX) at Lawrence Berkeley National Laboratory (LBNL) [10]. The image-charge effects have been found to play an important role when the maximum beam envelope reaches 80% of the pipe radius [1].

The purpose of this paper is to discuss the results of parametric studies based on the test-particle model. The percentage of beam loss to the conductor wall [2] is calculated as a function of propagating distance and aperture, and is compared to the simulation results from the particle-in-cell (PIC) code PFB2D.

DEPENDENCE OF THE IMAGE-CHARGE EFFECTS ON SYSTEM PARAMETERS

The halo formation and chaotic particle motion dependent sensitively on the system parameters: vacuum phase advance, the beam perveance, and the ratio of the beam size to the aperture [2].

The best way to illustrate the image charge effects on inducing chaotic particle motion and halo formation is to determine the boundary of regular motion region and chaotic sea, which is usually presented by a Kolmogorov-

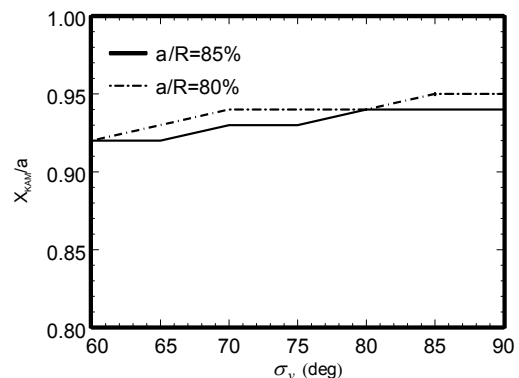


Figure 1: Plots of the relative outermost KAM surface location X_{KAM}/a as a function of the vacuum phase advance for $\eta = 0.5$, $KS/\varepsilon_x = 10.0$, $\varepsilon_x = \varepsilon_y = \varepsilon$ and two cases: (a) $a/R = 80\%$ and (b) $a/R = 85\%$.

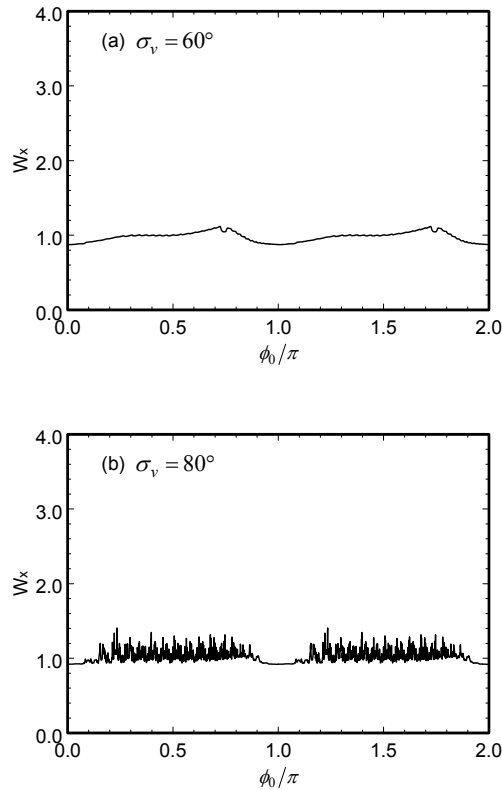


Figure 2: Plots of W_x vs ϕ_0 for 2000 test particles at axial distance $s/S = 50$ for $\eta = 0.5$, $KS/\varepsilon_x = 10.0$, $\varepsilon_x = \varepsilon_y = \varepsilon$, $a/R = 85\%$ and two cases: (a) $\sigma_v = 60^\circ$, and (b) $\sigma_v = 80^\circ$.

-Arnold-Moser (KAM) surface, as well as the rate of halo production which can be demonstrated by plotting the transverse energy for various initial conditions at certain axial distance.

As the vacuum phase advance decreases, the regular region of particle motion decreases, which means that for smaller vacuum phase advance more particles are in the chaotic sea and can form halo. As shown in Fig. 1, the KAM outermost surface location relative to the beam boundary, X_{KAM}/a , decreases as the vacuum phase advance decreases. However, the rate of the halo production decreases as the vacuum phase advance decreases. The locations and evolution of the chaotic particles are illustrated in Fig. 2, where the transverse energy $W_x(s/S = 50) = x^2/a^2 + (ax' - a'x)/\varepsilon^2$ is plotted for 2000 test particles loaded at $s = 0$ on the beam boundary $W_x(0) = 1$ in the phase space with the initial phases $\phi_0 = \tan^{-1}[(S/\varepsilon)^{1/2} a(0)x'(0)/x(0)]$ uniformly distributed from 0 to 2π for two cases: (a) $\sigma_v = 60^\circ$ and (b) $\sigma_v = 80^\circ$. Those regular particles remain inside the beam with $W_x \cong 1$, while the other test particles are chaotic and gain energy with $W_x > 1$. It is shown in Fig. 2

that for $\sigma_v = 80^\circ$ much more halo is formed with $W_x > 1$ than $\sigma_v = 60^\circ$ at $s/S = 50$.

Figures 3 and 4 show the dependence of the halo formation and chaotic particle motion on the beam perveance. As the perveance increases, the regular region

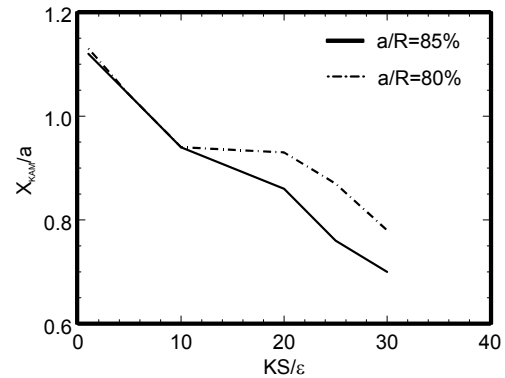


Figure 3: Plots of the relative outermost KAM surface location X_{KAM}/a as a function of the scaled perveance $\hat{K} = KS/\varepsilon$ for $\eta = 0.5$, $\varepsilon_x = \varepsilon_y = \varepsilon$, $\sigma_v = 80^\circ$ and two cases: (a) $a/R = 80\%$ and (b) $a/R = 85\%$.

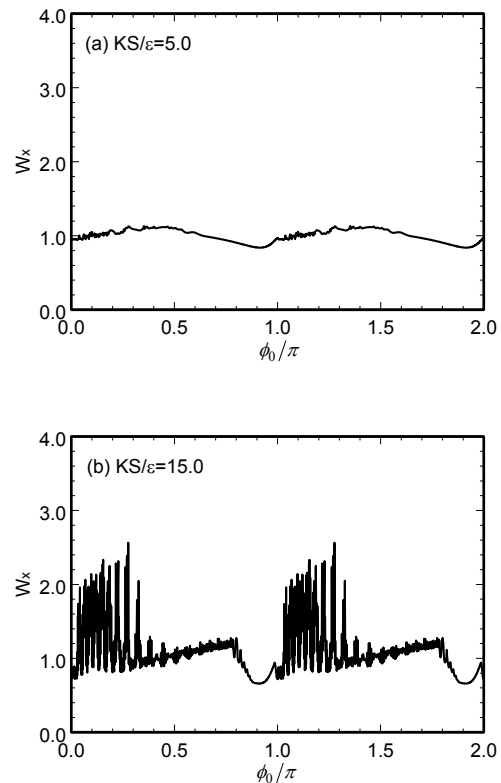


Figure 4: Plots of W_x vs ϕ_0 for 2000 test particles at axial distance $s/S = 50$ for $\eta = 0.5$, $\sigma_v = 80^\circ$, $\varepsilon_x = \varepsilon_y = \varepsilon$, $a/R = 85\%$ and two cases: (a) $KS/\varepsilon_x = 5.0$, and (b) $KS/\varepsilon_x = 15.0$.

of particle motion decreases, which means that for high intensity beam, more particles are in the chaotic sea. The rate of the halo production increases as the beam intensity increases. It is shown in Fig. 4 that the halo for $KS/\varepsilon_x = 15.0$ is more pronounced than that for $KS/\varepsilon_x = 5.0$ at $s/S = 50$.

Finally, the beam loss is computed as a function of propagation distance and pipe radius. As an example, the results are shown in Fig. 5 for HCX system parameter: $\eta = 0.5$, $KS/\varepsilon_x = 10.0$, $\varepsilon_x = \varepsilon_y = \varepsilon$ and $\sigma_v = 80^\circ$, and four choices of the pipe radius with $\hat{R} = R/\sqrt{\varepsilon S} = 3.8, 3.9, 4.0$, and 4.5 . The beam loss rate increases with the decreasing pipe radius, where the image effects play a more important role in the total space charge force. Although the results shown in Fig. 5 are based on the test-particle calculations, they provide order of magnitude estimates for the actual beam losses.

PIC SIMULATION

A particle-in-cell (PIC) code called Periodically Focused Beam 2D (PFB2D) is developed to study the beam loss induced by the image-charge effects. In the code, the beam distribution is presented by N macro-particles which are generated according to the KV distribution.

As shown in Fig. 6, the beam loss percentage is simulated by the PFB2D code for the parameter choice $\eta = 0.5$, $KS/\varepsilon_x = 10.0$, $\varepsilon_x = \varepsilon_y = \varepsilon$ and $\sigma_v = 60^\circ$, with the pipe radius $\hat{R} = 3.8$, where the dashed curve is calculated from the theory and solid curves are simulated by PFB2D with various choices of particle numbers. The beam loss is sensitive to the macro-particle number N . As N increases in the simulation, the result is closer to the theory prediction. Therefore, the noise in the PIC simulation for less particle number is significant, which will be a subject of future investigation.

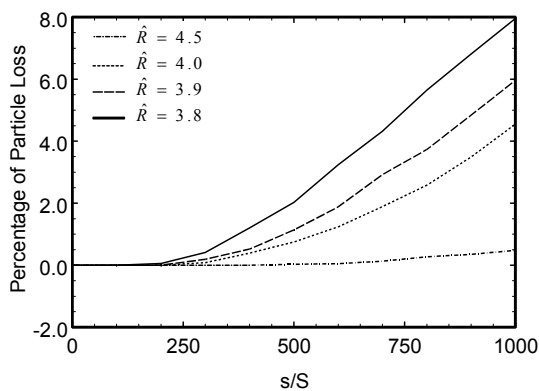


Figure 5: Plots of the percentage of particles striking the conductor wall as a function of propagation distance. Here, 10000 test particles with the KV distribution initially are used in the simulations.

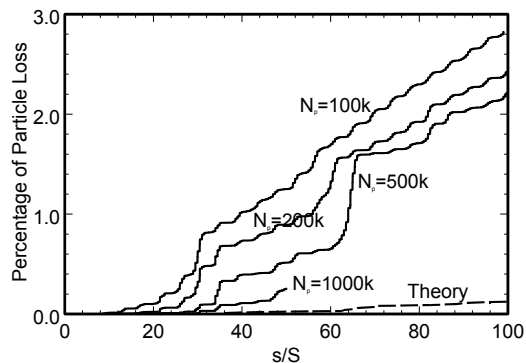


Figure 6: Plot of the beam loss percentage as a function of the propagating distance for $\hat{R} = 3.8$ and macro-particle number $N = 1 \times 10^5$, 2×10^5 , 5×10^5 , and 1×10^6 .

CONCLUSION

The dependence of image-charge effects on system parameters, such as the vacuum phase advance, the beam perveance and the ratio of the beam size to the aperture, was studied for the AG focusing system. The beam loss was calculated as a function of propagating distance and aperture, and is compared with simulation results from the particle-in-cell (PIC) code PFB2D. The noise in PIC simulation was found to be significant. It requires further investigation.

REFERENCES

- [1] J. Zhou, B. L. Qian, and Chiping Chen, *Physics of Plasma*, 10, P 4203 (2003).
- [2] J. Zhou and C. Chen, *Nucl. Instrum. and Methods in Phys. Res. A*, 544/1-2, pp. 492-496 (2005), in press.
- [3] R. L. Gluckstern, *Phys. Rev. Lett.* 73, 1247 (1994).
- [4] J. M. Lagniel, *Nucl. Instrum. Methods Phys. Res. A* 345, 405 (1994).
- [5] Q. Qian, R. C. Davidson, and C. Chen, *Phys. Plasmas* 2, 2674 (1995); *Phys. Rev. E* 51, R5216 (1995).
- [6] C. M. Celata, F. M. Bieniosek, L. Prost, et al., *Proc. of the 2003 Particle Accel. Conf., Portland, OR, May 2003* (IEEE, Piscataway, NJ, 2003).
- [7] R. W. Garnett, et al., in *Space Charge Dominated Beams and Applications of High Brightness Beams*, edited by S. Y. Lee, AIP Conf. Proc. No. 377 (AIP, New York, 1996), p. 60.
- [8] C. K. Allen, K. C. D. Chan, P. L. Colestock, et al., *Phys. Rev. Lett.* 89, 214802 (2002).
- [9] F. M. Bieniosek, J. W. Kwan, E. Henestroza, and C. Kim, *Nucl. Instrum. Methods Phys. Res. A* 464, 592 (2001).
- [10] P. A. Seidl, F. M. Bieniosek, C. M. Celata, et al., *Nucl. Instrum. Methods Phys. Res. A* 464, 369 (2001).
- [11] B. L. Qian, J. Zhou, and C. Chen, *Phys. Rev. ST Accel. Beams* 6, 014201 (2003).